ORIGINAL RESEARCH

Head and Neck Imaging

Comparing the double-echo steady-state with water excitation and constructive interference in steady state sequence techniques for identifying extracranial facial nerve and tumor positions in patients with parotid tumors

Xiaoxue Fan, Changwei Ding, Guyue Zhao, and Yang Hou

ABSTRACT

BACKGROUND AND PURPOSE: Reliable preoperative visualization of facial nerve morphology and understanding the spatial relationship between the facial nerve and tumor in the parotid gland can help clinicians perform safe and effective surgeries. Hence, this study aimed to compare the image quality of extracranial facial nerves obtained using double-echo steady-state with water excitation (DESS-WE) and constructive interference in steady state (CISS) sequences and evaluate their diagnostic efficacy in the localization of parotid tumors.

MATERIALS AND METHODS: In total, 32 facial nerves of 16 healthy volunteers and 25 facial nerves of 25 patients with parotid tumors were included in this retrospective study. All participants underwent noncontrast-enhanced extracranial facial nerve magnetic resonance imaging with DESS-WE and CISS with a 3T MR scanner equipped with a 64-channel head and neck coil. Image quality was subjectively evaluated using a 5-point Likert scale by two radiologists. Inter- and intra-rater agreements were assessed using the Cohen kappa coefficient (κ). Receiver operating characteristic analysis was performed, and the diagnostic efficacies of DESS-WE and CISS images in localizing parotid tumors were calculated.

RESULTS: For healthy volunteers (11 men and 5 women; median age, 26 years), image quality scores for CISS were significantly higher than those for DESS-WE for the discrimination of the temporofacial and cervicofacial trunks (both, $p < 0.001$). In patients with parotid tumors (12 men and 13 women; median age, 58 years), CISS performed better than DESS-WE in terms of visualizing the spatial relationship of the facial nerve to the tumor and diagnostic confidence (both, $p<0.001$). Regarding the localization of parotid tumors, CISS showed excellent performance, comparable to that of DESS-WE (area under the curve, 0.981 versus 0.942, $p = 0.1489$).

CONCLUSIONS: CISS achieved diagnostic performance comparable to DESS-WE in parotid tumor localization, with favorable image quality and more reliable morphological visualization of the facial nerve.

ABBREVIATIONS: 3D = three-dimensional; CISS = constructive interference in steady state; DESS-WE = double-echo steady-state with water excitation; IQS = image quality score; AUC = area under the curve.

From the Department of Radiology, Shengjing Hospital of China Medical University, Shenyang, China (X.F.; C.D.; G.Z.; Y.H.)

Received month day, year; accepted after revision month day, year.
From the Department of Radiology, Shengjing Hospital of China Medical University, Shenyang, China.

The authors declare no conflicts of interest related to the content of this article.

Please address correspondence to Yang Hou, PhD, Department of Radiology, Shengjing Hospital of China Medical University, Sanhao Street, Shenyang, 110004, China; houyang1973@163.com.

SUMMARY SECTION

PREVIOUS LITERATURE: DESS-WE images show the facial nerve trunk well in both healthy patients and patients with parotid tumors, and have high diagnostic accuracy for the localization of parotid tumors.

KEY FINDINGS: CISS images can be used for preoperative visualization of the extracranial facial nerve. CISS images provide reliable imaging of the location of the facial nerve relative to the lesion in patients with parotid tumors.

KNOWLEDGE ADVANCEMENT: CISS demonstrates better visualization of the facial nerve branches (temporofacial and cervicofacial trunks) compared with DESS-WE. Moreover, CISS is a reliablemethod for identifying the locations of parotid tumors.

INTRODUCTION

The standard treatment for parotid tumors is surgical resection, and facial nerve injury is one of the most serious complications associated with parotid surgery. [1-3] However, when the facial nerve is distorted and displaced owing to tumor compression, visual identification, which is usually reliable for facial nerve, becomes difficult. [4, 5] Even with intraoperative facial nerve monitoring, 2–6 % of patients develop permanent facial palsy after parotidectomy, [5-10] which severely affects their quality of life. Therefore, complete resection while preserving facial nerve function is the main goal of parotid tumor surgery.[2, 11] Notably, facial palsy is related to the location of the parotid tumor, more than 35% of patients with deep lobe tumors have been reported to develop temporary facial nerve palsy postoperatively; [12] and the rate of postoperative facial palsy is higher in patients with lesions involving the deep lobes than in those without;[2, 4, 10, 11] Surgery for deep lobe tumors of the parotid gland may require extensive circumferentially dissected peripheral nerve dissections; the increased extent of the facial nerve dissection may contribute to the temporary facial nerve palsy, leading to a higher incidence of permanent facial nerve palsy and consequently increasing the technical difficulty.[13] Therefore, accurate preoperative localization of the tumor and thoroughly explaining the potential risk of postoperative facial nerve palsy to patients are important clinical issues.

MR tractography has been used by head and neck specialists as a reliable and valid tool for identifying facial nerves. This technique can produce high-contrast anatomical atlases and is particularly reliable for identifying facial nerve contact points with parotid tumors.[14, 15] However, it is not ideal for visualizing uncompressed branches of facial nerves.[16] The reliable preoperative visualization of facial nerve morphology and understanding the spatial relationship between the facial nerve and tumor in the parotid gland can help clinicians perform safer and more effective surgeries.[17] Early preoperative identification of the course of the facial nerve provides more reliable images of the facial nerve and helps surgeons to safely and effectively resect tumors, avoid potentially harmful manipulations, and reduce mechanical trauma. Nonetheless, the reliable and direct observation of the extracranial segment of the facial nerve remains challenging.

High-resolution MR techniques, including a three-dimensional double-echo steady state water excitation (DESS-WE) sequence, have been attempted for direct visualization of the extracranial segment of the facial nerve and have been reported to have excellent performance.[18-20] DESS-WE sequence reportedly can reliably depict morphology of the extracranial segment of the facial nerve as well as the relationships to parotid tumors, with high diagnostic efficacy in terms of tumor localization;[19, 21, 22] however, this technique has limited ability in terms of visualizing the branches of the facial nerve. [19] The three-dimensional constructive interference in steady state (CISS) sequence, with its high resolution and clear visualization of small anatomical structures, has been widely used for the morphologic assessment of the facial and cochlear nerves in the internal auditory canal.[23] A study demonstrated that the CISS sequence can clearly show the temporofacial and cervicofacialbranches of the facial nerve; however, the number of patients with parotid tumors whose localizations were confirmed by surgery in that study was small (n = 3). [24]

Therefore, this study aimed to compare the quality of images obtained using DESS-WE and CISS sequences, compare their relative ability to show the extracranial segments of facial nerves, and evaluate their diagnostic efficacy in terms of the localization of parotid tumors.

MATERIALS AND METHODS

Ethics statements

This retrospective study was approved by our hospital's Institutional Review Board (No. 2023PS144J), and written informed consent was obtained from all participants.

Study Participants

From June 2022 to July 2023, volunteers and patients with parotid tumors were prospectively recruited. Healthy volunteers included participants aged ≥ 18 years. The exclusion criteria for the healthy volunteers were as follows: 1) history of head and neck tumors, 2) history of mumps, 3) history of head and neck surgery, 4) history of smoking, and 5) claustrophobia precluding MRI.

Patients with parotid tumors comprised participants who met the following inclusion criteria: 1) having undergone routine preoperative MR examination of the parotid gland and sequences of the extracranial segment of the facial nerve (including DESS-WE and CISS); 2) having received subsequent surgical treatment; 3) having detailed records of the location of the parotid tumor; and 4) age ≥ 18 years. Patients whose MRI studies had image quality deemed insufficient for diagnosis by radiologists were also excluded.

Imaging acquisition

All examinations were performed using a MAGNETOM Prisma 3.0 T MR scanner (Siemens Healthcare, Erlangen, Germany) equipped with a 64-channel head and neck coil. The detailed MR scan parameters of DESS-WE and CISS are provided in Table 1. Both DESS-WE and CISS sequence scans included the region from the stylomastoid foramen to the mandible; these two imaging sequences typically required approximately 20 minutes of acquisition time. In addition to the DESS-WE and CISS sequences, we obtained routine spin echo parotid MR images, including T1-weighted, T2-weighted, and T2WI fat-suppression images.

Table 1: Parameters for DESS-WE and CISS sequence.

Parameter	DESS-WE	CISS
TR (ms)	13.64	5.83
TE (ms)	4.68	2.57
Section thickness	0.5	0.5
Field of view (mm)	160×160	160×160
Matrix size	320×320	320×320
Voxel size (mm)	0.5×0.5×0.5	0.5×0.5×0.5
Band width (Hx/pixel)	315	504
Flip angle (°)	28	45
Acceleration method	PAT (GRAPPA)	-
Number of acceleration factor	2	-
Gradient times	80mT/m, 200 T/m/s	80mT/m, 200 T/m/s
Number of averages	1	1
Fat suppression	Water excit.	-
Number of slice	160	160
Acquistion time	7 min 39 s	10 min 18 s

CISS, constructive interference in steady state; DESS-WE, double-echo steady-state with water excitation; GRAPPA, generalized autocalibrating partially parallel acquisitions; PAT, Parallel acquisition technique

Quantitative Image Analysis

The original images were sent to the Intelligence Space Portal workstation (Netherlands) for quantitative image analysis. The regions of interest (ROI) used for the analysis in each region were drawn by two radiologists with 26 and 9 years of experience with parotid MR interpretation, respectively. The signal intensity of the extracranial segment of the main trunk of facial nerve was measured using an ovoid ROI of minimal size (1 mm^2). The short axis of the ellipse of the ROI should not exceed the extent of the facial nerve (Supplemental Figure). An ROI of the same size and same shape is placed on parotid tissue on the same image slice to measure its signal intensity, avoiding the area emcompassing blood vessels. The ROI for the background noise measured in the air was also selected on the same image slice of the same size and same shape as the facial nerve (Supplemental Figure). The ROI placement was consistently in its anatomic location, shape, and size across both DESS-WE and CISS sequences. The above quantitative data were measured separately by the two radiologists and analyzed using mean values. SNR was first calculated as follows: SNR_{fn} = mean signal intensity of facial nerve / standard deviation (SD) of background noise; SNR_{pp} = mean signal intensity of parotid parenchyma / SD of background noise. [25] Next, CNR was calculated between the facial nerve (SNR_{fn}) and parotid parenchyma (SNR_{pp}) as follows: CNR = SNR_{fn}-$SNR_{pp.}$ [26]

Qualitative Image Analysis

All images were uploaded to our picture archiving and communication system workstation (Neusoft PACS/RIS V5.5, Shenyang, China) for subsequent evaluation. The two radiologists independently scored the image quality using a 3D reconstruction post-processing function. The facial nerve showed a high signal on DESS-WE images and a low signal on CISS images. DESS-WE and CISS images were scored using a 5-point Likert scale in healthy volunteers and patients with parotid tumors. The parotid facial nerve exits from the stylomastoid foramen and then divides into the temporofacial and cervicofacial divisions in the parotid gland[19, 24]. In healthy volunteers, the visibility of the main trunk of the extracranial segment of the facial nerve and the proximal temporofacial and cervicofacial divisions were assessed on a reformatted sagittal oblique image that displays the main trunk and its bifurcation into the proximal temporofacial and cervicofacial divisions (Fig.1). In patients with parotid tumors, the clarity of tumor margin, the continuity of the facial nerve trunk from the foramen to the level of the parotid tumor, the spatial relationship between the facial nerve and the parotid tumor, and the diagnostic confidence level were each assessed on a scale of 1 to 5 (Table 2). For each of these parameters, an image quality score of ≥ 3 was considered satisfactory. The two radiologists reassessed the two sets of images for each patient again after at least 4 weeks to assess inter- and intra-rater agreements and avoid recall bias.

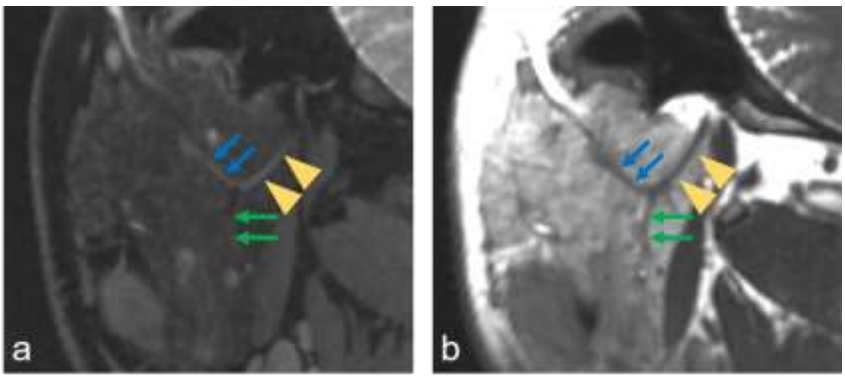

FIG 1. Standard observation slices for the image-based evaluation of the main, temporofacial, and cervicofacial trunks of the extracranial facial nerve of healthy volunteers in the oblique sagittal plane. The facial nerve shows a high signal on the DESS-WE image (a) and a low signal on the CISS image (b), with yellow arrowheads identifying the main trunk of the facial nerve, blue ones

identifying the temporofacial trunk, and green ones pointing out the cervicofacial trunk.

DESS-WE, double-echo steady-state with water excitation; CISS, constructive interference in steady state

Evaluation of the efficacy of parotid tumor localization

Parotid tumors were classified into two subgroups on the basis of Kim et al.'s [19] criteria: (1) deep lobe -, tumors not involving the deep lobe, and located exclusively lateral to the facial nerve; and (2) deep lobe +, tumors involving the deep lobe, including those exclusively medial to the facial nerve, or have components both medial and lateral to the facial nerve. Radiologists used the multiplanar postprocessing function to assess the spatial relationship between the extracranial facial nerve and the parotid tumor on DESS-WE and CISS images, for localization (Fig. 2). For each lesion, the two radiologists made independent diagnoses, and both were blinded to the patient's surgical data or results. The diagnostic efficacy of DESS-WE and CISS images for determining whether a tumor is deep lobe - or deep lobe + was assessed using the relative location of the facial nerve and the parotid tumor as seen during surgery, which is currently considered to be the reference standard.

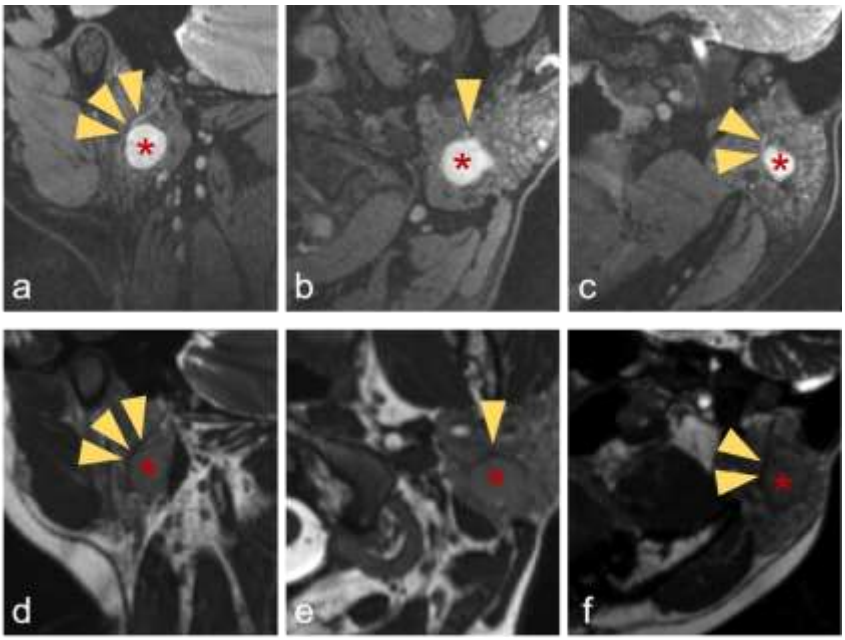

FIG 2. Image quality assessment of parotid tumors. Representative images of the clarity of tumor lesions in DESS-WE sequence (a-c) and CISS sequence (d-f); the continuity of the facial nerve to the level of the tumor in the oblique sagittal plane (a, d); the relative position of the facial nerve to the tumor and the diagnostic confidence of the tumor localization in the oblique sagittal (a, d), transverse (b, e), and oblique coronal planes (c, f); yellow arrowheads identify the main trunk of the facial nerve, and red asterisks (*) denote the tumor.

DESS-WE, double-echo steady-state with water excitation; CISS, constructive interference in steady state

Statistical analysis

Non-normally distributed variables are presented as medians. The Wilcoxon signed-rank test was used to compare the image quality score (IQS) of DESS-WE and CISS images. After testing the normality of continuous variables using the Shapiro-Wilk test, normally distributed variables are represented by the mean value ± standard deviation. Inter- and intra-rater agreements for the IQS were evaluated using the Cohen kappa coefficient (κ). The weighted kappa coefficient (κ) was defined as follows: poor (0.00–0.20); fair (0.21–0.40); moderate (0.41–0.60); good (0.61–0.80); and excellent (0.81–1.00).[27, 28] If the two radiologists' subjective evaluation of the IQS showed good agreement (κ value > 0.60), the IQS of the more senior radiologist is used as the final IQS for comparison in order to simplify scoring. The accuracy, sensitivity, and specificity of the DESS-WE and CISS image data were calculated, and the diagnostic efficacies of the two sets of images were compared using receiver operating characteristic analysis. All data were analyzed using SPSS software version 26.0 (IBM Corp., Armonk, NY, USA) and MedCalc® Statistical Software version 19.6 (MedCalc Software Ltd., Ostend, Belgium). A p-value of < 0.05 was considered statistically significant.

RESULTS

Patient characteristics

In total, 16 healthy volunteers (11 men and 5 women; median age, 26 years; age range, 19–71 years) were enrolled. Hence, 32 facial nerves (2 per healthy volunteer) were imaged. Twenty-eight patients with parotid tumors met the inclusion criteria, of whom three were excluded: two because of severe swallowing artifact on MR imagesand one because the facial nerve location could not be accurately confirmed surgically owing to the aspiration of cyst contents altering anatomic configuration of the tumor and regional structures. Hence, the final

cohort comprised 25 patients (12 men and 13 women; median age, 58 years; range, 28–84 years) with a total of 30 parotid tumors: 3 ipsilateral Warthin tumors in 1 patient, 2 bilateral Warthin tumors in 2 patients, and 1 small cell carcinoma and 1 ipsilateral lymph node metastasis in 1 patient) (Supplemental Table 1).

Quantitative comparison of DESS-WE and CISS images

The SNR_{fn} was significantly lower in DESS-WE images than in CISS images (p value < 0.001 for all; Table 3). In addition, regarding analysis of the obtained CNR, the CNR of the CISS image was significantly higher than that of the DESS-WE image in all analyzed participants (healthy volunteers and patients; p value < 0.001 for all; Table 3).

Table 3: SNR and CNR of DESS-WE and CISS.

	Participants	DESS-WE (mean ± SD, range)	CISS (mean ± SD, range)	p
SNR				
	Healthy volunteers	17.14 ± 3.19 (9.42–21.99)	49.81 ± 11.27 (29.65–73.27)	**<0.001**
	Patients	17.13 ± 5.00 (8.27–26.34)	46.85 ± 14.11 (30.26–102.45)	**<0.001**
	Overall	17.14 ± 4.13 (8.27–26.34)	48.38 ± 12.70 (29.65–102.45)	**<0.001**
CNR				
	Healthy volunteers	7.07 ± 2.39 (2.88–11.73)	54.10 ± 17.07 (25.18–91.20)	**<0.001**
	Patients	7.26 ± 3.65 (1.49–14.83)	50.45 ± 13.39 (29.39–80.24)	**<0.001**
	Overall	7.21 ± 2.94 (1.49–14.83)	52.33 ± 15.38 (24.18–91.20)	**<0.001**

CISS, constructive interference in steady state; CNR, contrast-to-noise ratio; DESS-WE, double-echo steady-state with water excitation; SNR, signal-to-noise ratio

Subjective evaluation of DESS-WE and CISS images in healthy volunteers

In the healthy volunteers, good inter- and intra-rater agreements for IQS (κ = 0.724–0.816) were observed (Table 4). Both radiologists could distinguish the facial nerve trunk well on DESS-WE and CISS images; however, the IQS of facial nerve trunk visibility on CISS images (median: 5, IQR: 4–5) was higher than that on DESS-WE images (median: 4, IQR: 4–5) (p = 0.061). Using the level of facial nerve bifurcation as the reference, although both radiologists were able to clearly distinguish the two main branches on both sequences, the IQSs of CISS for the temporofacial (median: 4, IQR: 4–4) and cervicofacial (median: 4, IQR: 4–4) division displays were significantly higher than those of DESS-WE for the temporofacial (median: 3, IQR: 3–4) and cervicofacial (median: 3, IQR: 3–4) division displays (p <0.001; Fig.3 and Supplemental Table 2).

Table 4: Intra- and inter-rater agreements for the image quality of DESS-WE and CISS.

	Participants	Segmentation	DESS-WE	CISS
Inter-rater kappa (95% CI)	Healthy volunteers	Facial nerve trunk visibility	0.724 (0.477-0.971)	0.796 (0.660-0.994)
		Temporofacial trunk visibility	0.753 (0.533-0.972)	0.816 (0.644-0.988)
		Cervicofacial trunk visibility	0.738 (0.522-0.954)	0.809 (0.635-0.983)
Intra-rater kappa (95% CI)	Healthy volunteers	Facial nerve trunk visibility	0.740 (0.503-0.977)	0.783 (0.580-0.995)
		Temporofacial trunk visibility	0.759 (0.553-0.966)	0.805 (0.623-0.986)
		Cervicofacial trunk visibility	0.728 (0.487-0.968)	0.755 (0.557-0.952)
Inter-rater kappa (95% CI)	Patients	Clarity of tumor margin	0.841 (0.692-0.989)	0.797 (0.625-0.968)
		Continuity	0.810 (0.646-0.974)	0.774 (0.551-0.997)
		Spatial relationship	0.793 (0.624-0.963)	0.784 (0.575-0.993)
		Diagnostic confidence	0.784 (0.638-0.931)	0.780 (0.566-0.994)
Intra-rater kappa (95% CI)	Patients	Clarity of tumor margin	0.817 (0.651-0.982)	0.763 (0.584-0.943)
		Continuity	0.794 (0.604-0.982)	0.757 (0.568-0.946)
		Spatial relationship	0.854 (0.726-0.983)	0.779 (0.563-0.996)
		Diagnostic confidence	0.870 (0.750-0.989)	0.786 (0.584-0.989)

IQS, image quality score; DESS-WE, double-echo steady-state with water excitation; CISS, constructive interference in steady state; Continuity: Continuity of the facial nerve trunk from the foramen to the level of the parotid tumor; Spatial relationship: the relative position of the facial nerve in relation to the tumor

Subjective evaluation of DESS-WE and CISS images in patients with parotid tumors

In patients with parotid tumors, subjective evaluation of the quality of the two sets of images by the two radiologists showed good agreement, with κ values > 0.750 (Table 4). Although the score of the clarity of tumor margin was lower on CISS (median: 4, IQR: 3–4) than on DESS-WE (median: 4, IQR: 3.75–4) (p = 0.018), both techniques scored well in terms of the continuity of the main trunk of the facial nerve from the foramen to the level of the parotid tumor, without statistically significant differences between DESS-WE (median: 4, IQR: 4–5) and CISS (median: 5, IQR: 4–5) (p = 0.083), The scores in terms of visualizing the spatial relationships between tumors and facial nerves, and the level of diagnostic confidence, were both higher for CISS than for DESS (both p < 0.001; Fig. 3 and Supplemental Table 2). However, in three patients, diagnostic confidence was scored as < 3 owing to large tumor sizes that resulted in poor visualization of the spatial relationship between the tumor and facial nerve on DESS-WE images.

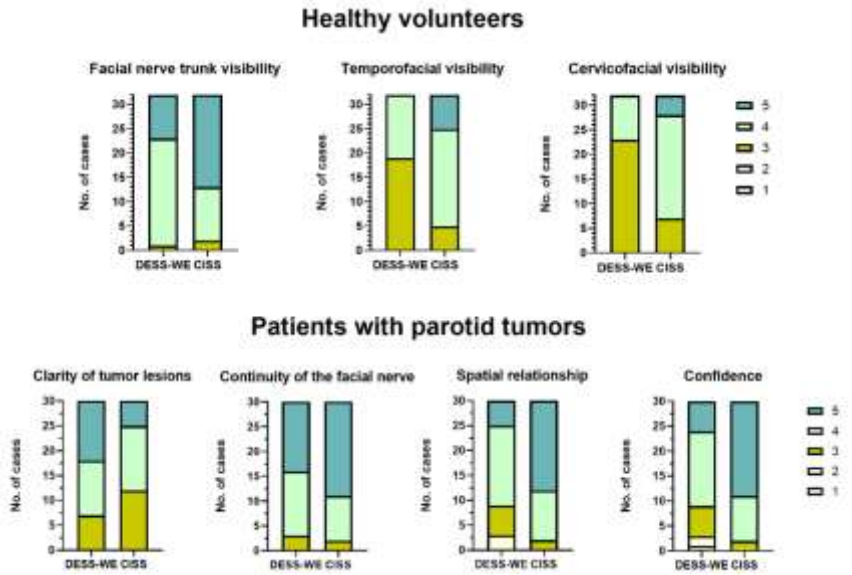

FIG 3. Subjective evaluation of the quality of DESS-WE and CISS images. All subgroups, including 16 healthy volunteers (32 facial nerves) and 25 patients (30 parotid tumors) were scored on a 5-point scale for multiple parameters, with scores of > 3 indicating satisfactory quality and scores of 1–2 score indicating unsatisfactory quality.

DESS-WE, double-echo steady-state with water excitation; CISS, constructive interference in steady state

Evaluation of the diagnostic efficacy of parotid tumor localization

Surgical findings confirmed that 26 lesions were localized to the superficial lobe, whereas 4 had components involving the deep lobe. The areas under the curve (AUCs) in terms of parotid tumor localization using DESS-WE and CISS were 0.942 (95% CI, 0.792–0.994) and 0.981 (95% CI, 0.850–1.000), respectively. Both, therefore, represented excellent methods for the purpose; there was no significant difference between the two (p = 0.1489; Table 5).

Table 5: Visibility of the DESS-WE and CISS images for the localization of parotid tumors (n = 30).

Imaging findings	Surgical findings		Diagnostic performance			
	deep lobe +	deep lobe -	AUC (95% CI)	Accuracy	Sensitivity	Specificity
DESS-WE						
deep lobe +	4	3	0.942 (0.792-0.994)	90%	100%	88.5%
deep lobe -	0	23				
CISS						
deep lobe +	4	1	0.981 (0.850-1.000)	96.7%	100%	96.2%
deep lobe -	0	25				
p	0.1489					

DESS-WE, double-echo steady-state with water excitation; CISS, constructive interference in steady state; AUC, area under the curve

DISCUSSION

The results of this study indicated that CISS had better performance in identifying intraparotid facial nerve branches compared with DESS-WE. Specifically, CISS can show the spatial relationship between intraparotid facial nerve and parotid tumor with excellent agreement with intraoperative findings and can satisfy the requirements for preoperative surgical planning.

As has been shown previously, DESS-WE images are able to trace the facial nerve trunk and show a high level of accuracy (Kim et al. [19], 92% vs. Fujii et al. [21], 97.8%) for localizing deep lobe tumors in patients with parotid tumors [19, 21]—a finding that is consistent with our results. However, the overall accuracy of localizing deep lobe tumors in this study was lower than what was reported in an earlier study by Fujii et al. (97.8%), [21] possibly because they included more deep lobe lesions (25.2%). Although we had fewer deep lobe tumors (13.3%), the proportion observed in our study is in line with the reported incidence of deep lobe tumors in the parotid gland (10%). [29] We observed that CISS images were as effective for localizing parotid tumors as DESS-WE images, which is also consistent with the findings of Guenette et al. [24] (100%). Although the CISS images scored lower in terms of the clarity of visualized tumors, CISS images scored higher in terms of the relative position of the facial nerve to the tumor. The relative position of the facial nerve to the tumor is the major concern from the surgeon's viewpoint,[11, 30, 31] because this can most affect the time needed for surgery, as well as postoperative facial function and aesthetics. The secondary branches of the intraparotid facial nerve (temporal, zygomatic, buccal, marginal mandibular, cervical) in patients with parotid tumors were not explored in this study, mainly because the surgeon's first step during parotid surgery is typically to identify the facial nerve trunk proximal to the tumor. Parotid tumors located superior to the main trunk of the facial nerve have a significantly higher risk of facial nerve injury, [32] and accurate identification of the main trunk of the facial nerve is a major factor in the attempt to avoid postoperative facial nerve injury. [10] Therefore, observation of the trunk of the facial nerve was most important for surgical planning in most cases.

For three of our patients with parotid tumors, there was low diagnostic confidence in the DESS-WE sequences. This may be because, in DESS-WE sequences, both the facial nerves and the tumors had high signal intensity. [26] Therefore, when the tumor was close to the facial nerve, there was less parotid parenchyma and little contrast distinction between them, [21] making it difficult to determinethe boundary

between the two. This study also noted that the CNR of DESS-WE images was lower than that of CISS images, which is consistent with the the findings of Hilgenfeld T et al.[33]. In patients with parotid tumors, CISS images were better than DESS-WE images in terms of visualizing the spatial relationship between the facial nerve and the tumor; therefore, even if the tumor is close to the facial nerve, the spatial relationship between the two can be clearly observed using CISS.

We also observed that, normal parotid glands without tumor, DESS-WE sequences had excellent performance regarding the facial nerve trunk. For the branches of the facial nerve (i.e., the temporofacial and cervicofacial divisions), only limited assessments could be performed using DESS-WE images; [19] however, CISS images with high CNR showed more details of the facial nerve branches in the parotid gland and are more reliable for preoperative planning and enhancing clinician confidence in the surgical plans. These findings may have immediate implications for the performance of facial nerve MRI.

The DESS sequence involves the acquisition of two different echoes during each repetition time, formed from FISP and reversed fast imaging with steady-state precession (PSIF) DWI sequence signals separately, which are then combined to form a single image. [34] The former provides more anatomical detail, whereas the latter the accentuates the signal intensity with strong T2 contrast. [34] Meanwhile, combining the WE technique with the DESS sequence can clearly show the facial nerve itself without relying on the fatty tissue background.[35] In addition, the CISS sequence can differentiate between fat and parotid parenchyma, has high spatial resolution and high SNR, and is relatively insensitive to motion; [34] this enables visualization of the extracranial facial nerve branches in the parotid gland, providing remarkable anatomical detail. [36] In this study, both DESS-WE and CISS images were able to identify the temporofacial and cervicofacial branches with good agreement, which is consistent with the findings ($\kappa > 0.70$) of Jeong et al. [22].

This study has some limitations. First, this study included a small number of patients with deep lobe tumors (n = 4), it did not have a high statistical power, and it evaluated only the localization of the relationship between the main trunk of facial nerveand parotid lesions—with the clinical outcomes of the parotidectomy procedures not being compared between the patients. Second, only patients with first-time parotid tumors were included when we evaluated the visualization of the facial nerve, and patients with recurrence were not evaluated. As the surgical field is affected by scarring and fibrosis, identification of the facial nerve can become difficult. If the nerve can be identified during surgery for recurrent parotid tumors, the probability of successful preservation of the facial nerve is high.[10] Lastly, this study only compares two sequences - CISS and DESS-WE, but PSIF and contrast-enhanced short-tau inversion recovery sequences also have good distinction of facial nerve, which were not simultaneously incorporated to the qualitative and quantitative analyses to determine the optimal protocol for examination of the extracranial segment of the facial nerve.

CONCLUSIONS

CISS achieved a diagnostic performance comparable to that of DESS-WE in terms of parotid tumor localization, with favorable image quality but more reliable morphological visualization of the facial nerve. CISS images can provide surgeons with anatomical information regarding parotid tumors and facial nerves, alleviate the problem of facial nerve identification, and assist clinicians in planning optimal surgical approaches.

ACKNOWLEDGMENTS

We wish to thank our colleagues in the Radiology and Dental Departments who collaborated with us in the preparation of the manuscript.

REFERENCES

1. Park W, Park J, Park S I, et al. Clinical outcomes and management of facial nerve in patients with parotid gland cancer and pretreatment facial weakness. *Oral Oncol* 2019;89:144-9.https://doi.10.1016/j.oraloncology.2019.01.003
2. Kawata R, Kinoshita I, Omura S, et al. Risk Factors of Postoperative Facial Palsy for Benign Parotid Tumors: Outcome of 1,018 Patients. *Laryngoscope* 2021;131:E2857-E64.https://doi.10.1002/lary.29623
3. Bittar R F, Ferraro H P, Ribas M H, et al. Facial paralysis after superficial parotidectomy: analysis of possible predictors of this complication. *Braz J Otorhinolaryngol* 2016;82:447-51.https://doi.10.1016/j.bjorl.2015.08.024
4. Olsen K D, Quer M, De Bree R, et al. Deep lobe parotidectomy-why, when, and how? *Eur Arch Otorhinolaryngol* 2017;274:4073-8.https://doi.10.1007/s00405-017-4767-5
5. Saadya A, Chegini S, Morley S, et al. Augmented reality presentation of the extracranial facial nerve: an innovation in parotid surgery. *Br J Oral Maxillofac Surg* 2023;61:428-36.https://doi.10.1016/j.bjoms.2023.05.007
6. Ruohoalho J, Makitie A A, Aro K, et al. Complications after surgery for benign parotid gland neoplasms: A prospective cohort study. *Head Neck* 2017;39:170-6.https://doi.10.1002/hed.24496
7. Hohman M H, Bhama P K, Hadlock T A. Epidemiology of iatrogenic facial nerve injury: a decade of experience. *Laryngoscope* 2014;124:260-5.https://doi.10.1002/lary.24117
8. Jin H, Kim B Y, Kim H, et al. Incidence of postoperative facial weakness in parotid tumor surgery: a tumor subsite analysis of 794 parotidectomies. *BMC Surg* 2019;19:199.https://doi.10.1186/s12893-019-0666-6
9. Sood A J, Houlton J J, Nguyen S A, et al. Facial nerve monitoring during parotidectomy: a systematic review and meta-analysis. *Otolaryngol Head Neck Surg* 2015;152:631-7.https://doi.10.1177/0194599814568779
10. Kuriyama T, Kawata R, Higashino M, et al. Recurrent benign pleomorphic adenoma of the parotid gland: Facial nerve identification and risk factors for facial nerve paralysis at re-operation. *Auris Nasus Larynx* 2019;46:779-84.https://doi.10.1016/j.anl.2019.02.010
11. Kinoshita I, Kawata R, Higashino M, et al. Tumor localization is the important factor for recovery time of postoperative facial nerve paralysis in

benign parotid surgery. *Auris Nasus Larynx* 2023.https://doi.10.1016/j.anl.2023.07.002
12. Aasen M H, Hutz M J, Yuhan B T, et al. Deep Lobe Parotid Tumors: A Systematic Review and Meta-analysis. *Otolaryngol Head Neck Surg* 2022;166:60-7.https://doi.10.1177/01945998211009235
13. Zenga J, Lin B M, Chen J, et al. Microsurgical instrument-assisted facial nerve dissection for deep lobe parotid tumors. *Laryngoscope* 2018;128:2529-31.https://doi.10.1002/lary.27188
14. Attye A, Karkas A, Tropres I, et al. Parotid gland tumours: MR tractography to assess contact with the facial nerve. *Eur Radiol* 2016;26:2233-41.https://doi.10.1007/s00330-015-4049-9
15. Castellaro M, Moretto M, Baro V, et al. Multishell Diffusion MRI-Based Tractography of the Facial Nerve in Vestibular Schwannoma. *AJNR Am J Neuroradiol* 2020;41:1480-6.https://doi.10.3174/ajnr.A6706
16. Rouchy R C, Attye A, Medici M, et al. Facial nerve tractography: A new tool for the detection of perineural spread in parotid cancers. *Eur Radiol* 2018;28:3861-71.https://doi.10.1007/s00330-018-5318-1
17. Hussain T, Nguyen L T, Whitney M, et al. Improved facial nerve identification during parotidectomy with fluorescently labeled peptide. *Laryngoscope* 2016;126:2711-7.https://doi.10.1002/lary.26057
18. Chu J, Zhou Z, Hong G, et al. High-resolution MRI of the intraparotid facial nerve based on a microsurface coil and a 3D reversed fast imaging with steady-state precession DWI sequence at 3T. *AJNR Am J Neuroradiol* 2013;34:1643-8.https://doi.10.3174/ajnr.A3472
19. Kim Y, Jeong H S, Kim H J, et al. Three-dimensional double-echo steady-state with water excitation magnetic resonance imaging to localize the intraparotid facial nerve in patients with deep-seated parotid tumors. *Neuroradiology* 2021;63:731-9.https://doi.10.1007/s00234-021-02673-3
20. Zhao Y, Yang B. Value of Visualization of the Intraparotid Facial Nerve and Parotid Duct Using a Micro Surface Coil and Three-Dimensional Reversed Fast Imaging With Steady-State Precession and Diffusion-Weighted Imaging Sequence. *J Craniofac Surg* 2018;29:e754-e7.https://doi.10.1097/SCS.0000000000004704
21. Fujii H, Fujita A, Kanazawa H, et al. Localization of Parotid Gland Tumors in Relation to the Intraparotid Facial Nerve on 3D Double-Echo Steady-State with Water Excitation Sequence. *AJNR Am J Neuroradiol* 2019;40:1037-42.https://doi.10.3174/ajnr.A6078
22. Jeong H S, Kim Y, Kim H J, et al. Imaging of Facial Nerve With 3D-DESS-WE-MRI Before Parotidectomy: Impact on Surgical Outcomes. *Korean J Radiol* 2023;24:860-70.https://doi.10.3348/kjr.2022.0850
23. Ozdemir M, Kavak R P. Morphometric analysis of facial and cochlear nerves in normal-hearing ears using 3D-CISS. *J Otol* 2019;14:136-40.https://doi.10.1016/j.joto.2019.05.004
24. Guenette J P, Ben-Shlomo N, Jayender J, et al. MR Imaging of the Extracranial Facial Nerve with the CISS Sequence. *AJNR Am J Neuroradiol* 2019;40:1954-9.https://doi.10.3174/ajnr.A6261
25. Guenette J P, Seethamraju R T, Jayender J, et al. MR Imaging of the Facial Nerve through the Temporal Bone at 3T with a Noncontrast Ultrashort Echo Time Sequence. *AJNR Am J Neuroradiol* 2018;39:1903-6.https://doi.10.3174/ajnr.A5754
26. Qin Y, Zhang J, Li P, et al. 3D double-echo steady-state with water excitation MR imaging of the intraparotid facial nerve at 1.5T: a pilot study. *AJNR Am J Neuroradiol* 2011;32:1167-72.https://doi.10.3174/ajnr.A2480
27. Landis Jr K G. The measurement of observer agreement for categorical data. *Biometrics* 1977;33:159-74
28. Benchoufi M, Matzner-Lober E, Molinari N, et al. Interobserver agreement issues in radiology. *Diagn Interv Imaging* 2020;101:639-41.https://doi.10.1016/j.diii.2020.09.001
29. Harney M S, Murphy C, Hone S, et al. A histological comparison of deep and superficial lobe pleomorphic adenomas of the parotid gland. *Head Neck* 2003;25:649-53.https://doi.10.1002/hed.10281
30. Kim J K, Lee D W, Geum S, et al. Ultrasonographic Localization of Parotid Gland Tumor Relative to the Facial Nerve Using Stensen's Duct Criterion. *J Oral Maxillofac Surg* 2023;81:1055-61.https://doi.10.1016/j.joms.2023.05.012
31. El Kininy W, Roddy D, Davy S, et al. Magnetic resonance diffusion weighted imaging using constrained spherical deconvolution-based tractography of the extracranial course of the facial nerve. *Oral Surg Oral Med Oral Pathol Oral Radiol* 2020;130:e44-e56.https://doi.10.1016/j.oooo.2019.12.012
32. Chiesa-Estomba C M, Echaniz O, Sistiaga Suarez J A, et al. Machine Learning Models for Predicting Facial Nerve Palsy in Parotid Gland Surgery for Benign Tumors. *J Surg Res* 2021;262:57-64.https://doi.10.1016/j.jss.2020.12.053
33. Hilgenfeld T, Saleem M A, Schwindling F S, et al. High-Resolution Single Tooth MRI With an Inductively Coupled Intraoral Coil-Can MRI Compete With CBCT? *Invest Radiol* 2022;57:720-7.https://doi.10.1097/RLI.0000000000000890
34. Chavhan Gb B P, Jankharia Bg, Cheng Hl, Shroff Mm. Steady-state MR imaging sequences: physics, classification, and clinical applications. *Radiographics*;28:1147-60.https://doi.10.1148/rg.284075031
35. Eckstein F, Hudelmaier M, Wirth W, et al. Double echo steady state magnetic resonance imaging of knee articular cartilage at 3 Tesla: a pilot study for the Osteoarthritis Initiative. *Ann Rheum Dis* 2006;65:433-41.https://doi.10.1136/ard.2005.039370
36. Wen J, Desai N S, Jeffery D, et al. High-Resolution Isotropic Three-Dimensional MR Imaging of the Extraforaminal Segments of the Cranial Nerves. *Magn Reson Imaging Clin N Am* 2018;26:101-19.https://doi.10.1016/j.mric.2017.08.007

Table 2: Subjective evaluation of the image quality score of the two sequences.

Score	Healthy volunteers			Patients			
	Facial nerve trunk visibility	Temporofacial division visibility	Cervicofacial division visibility	Clarity of tumor margin	Continuity	Spatial relationship	Diagnostic confidence
1	No contrast with surrounding tissue	No contrast with surrounding tissue	No contrast with surrounding tissue	No evident boundaries	Discontinuous display with linear deficiency	Indistinguishable, not acceptable for assessment	Very poor
2	Nerve display discontinuity, blurred lines	Proximal nerve discontinuity, blurred lines	Proximal nerve discontinuity, blurred lines	More than 50% circumference margin blurring	Intermittent display with dotted deficiency	Blurred boundaries, moderately limited assessment	Lack of confidence
3	Identifiable with uneven thickness	Proximal recognizable with uneven thickness	Proximal recognizable with uneven thickness	20%–50% circumference margin blurring	Continuously visible with uneven thickness	Demarcation is identifiable, with mild limitations in assessment	Diagnosis is possible
4	Clear recognition, moderate thickness	Proximal clear recognition, moderate thickness	Proximal clear recognition, moderate thickness	Less than 20% circumference margin blurring	Full length visible with mild thickness fluctuations	Boundary edges visible, few constraints on assessment	Good
5	Clear recognition, constant thickness	Nerve contrast is obvious, with constant thickness	Nerve contrast is obvious, with constant thickness	Full circumference clearly visible	Full length visible with constant thickness	Clear boundary	Very good

Continuity: Continuity of the facial nerve trunk from the foramen to the level of the parotid tumor; Spatial relationship: the relative position of the facial nerve in relation to the tumor

SUPPLEMENTAL FILES

Supplemental Table 1: Histologic typesof parotid lesions (n=30).

Histologic Types	n (%)
Benign tumors	
Pleomorphic adenoma	7 (23.3%)
Warthin tumor	13 (43.3%)
Cyst	2 (6.7%)
Eosinophilic papillary cystadenoma	2 (6.7%)
Monomorphic adenoma	1 (3.3%)
Ductal papilloma	1 (3.3%)
Malignant tumors	
Metastatic tumor	1 (3.3%)
Acinic cell carcinoma	1 (3.3%)
Mucoepidermoid carcinoma	1 (3.3%)
Small cell carcinoma	1 (3.3%)

Supplemental Table 2: Image Quality Score of DESS-WE and CISS sequences.

Participants	Segmentation	Median (IQR) DESS-WE	Median (IQR) CISS	p
Healthy volunteers	Facial nerve trunk visibility	4 (4-5)	5 (4-5)	0.061
	Temporofacial trunk visibility	3 (3-4)	4 (4-4)	**<0.001**
	Cervicofacial trunk visibility	3 (3-4)	4 (4-4)	**<0.001**
Patients	Clarity of tumor margin	4 (3.75-5)	4 (3-4)	**0.018**
	Continuity	4 (4-5)	5 (4-5)	0.083
	Spatial relationship	4 (3-4)	5 (4-5)	**<0.001**
	Diagnostic confidence	4 (3-4)	5 (4-5)	**<0.001**

CISS, constructive interference in steady state; DESS-WE, double-echo steady-state with water excitation; IQS, image quality score; IQR, interquartile range.

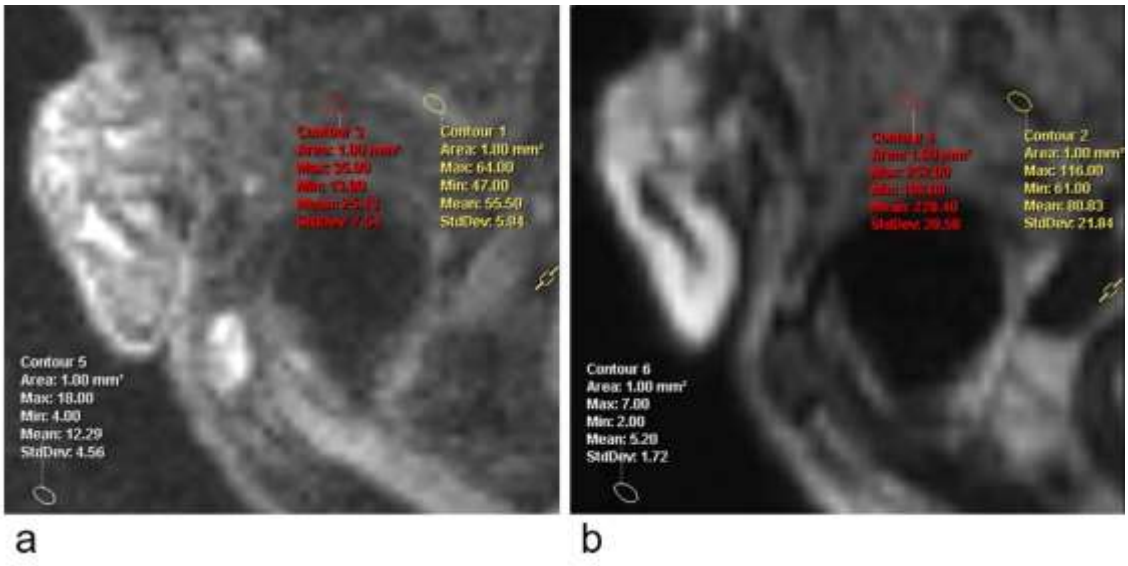

Supplemental Figure. Drawing of the ROI inside the region and measuring the mean signal intensity of facial nerve, mean signal intensity of parotid parenchyma, and standard deviation of background noise. The ROI placement was consistently in its anatomic location, shape, and size across both axial DESS-WE (a) and CISS (b) sequences. A 1 mm^2 ROI was marked and the short axis of the ellipse of the ROI within the internal border of facial nerve (yellow ovoid); ROIs for the parotid parenchyma(red ovoid) and background noise (white ovoid) are also placed on the same image slice, using the same size and same shape, and ensuring that the parotid parenchyma ROI avoiding the blood vessels.

DESS-WE, double-echo steady-state with water excitation; CISS, constructive interference in steady state